Superconducting properties of perforated NbN films using ordered arrays of ferromagnetic nanowires

X. Hallet,[1,*] S. Adam,[1] L. Piraux,[1] J. Vanacken,[2] and V. V. Moshchalkov[2]

[1]*Institute of Condensed Matter and Nanosciences, Université catholique de Louvain (UCL), Place Croix du Sud 1, BE-1348 Louvain-la-Neuve, Belgium*

[2]*Institute for Nanoscale Physics and Chemistry, Katholieke Universiteit Leuven (KUL), Celestijnenlaan 200D, BE-3001 Leuven, Belgium*

(Received 29 June 2011; published 31 October 2011)

The superconducting properties of NbN thin films deposited perpendicularly and embedding a 100-nm-spaced triangular array of ferromagnetic nanowires have been studied. Matching effects are found to persist up to 3 T in these superconductor-ferromagnet hybrids. Other interesting matching features have been also observed. The first matching field depends on the magnetic history. It can be shifted practically at will between the theoretical matching field H_1 and a lower field H_1^* that depends on the shape of the magnetization hysteretic loop of the nanowires array. Therefore, this shift is strongly influenced by the nanowires packing, in particular by the nanowires diameter in the present system. The reduction of the first matching field is associated with an enhancement of the superconducting state that is the strongest when the first matching field is shifted down to H_1^*. Finally, misleading field-induced superconductivity has been observed in fields up to 1.2 T.

DOI: 10.1103/PhysRevB.84.144529 PACS number(s): 74.25.Wx, 74.25.Ha, 74.25.F−

I. INTRODUCTION

Superconductor-ferromagnet hybrids are very interesting systems due to the antagonism between the antiparallel spin alignment in the superconducting state and the parallel spin alignment in the ferromagnet (for a review, see Buzdin).[1] The magnetic interaction between the magnetic domains of the ferromagnet and the superconducting vortices has also attracted much attention over the past years (for a review see Refs. 2–5). For this purpose, the ferromagnet is separated from the superconductor by a thin insulating layer so only the magnetic interaction is involved. The way has been paved by Otani and coworkers[6] who used a GdCo dots array on top of a Nb film in which the magnetization of the dots was in-plane (i.e., parallel to the superconducting film). The stray magnetic fields of the magnetic dots were acting as pinning centers for the vortices. Since then, many experimental[7–17] and theoretical[18–21] works have been performed. Notably, Hoffmann *et al.*[8] compared experimentally the vortex pinning in superconducting films deposited on top of square arrays of magnetic and nonmagnetic dots of different sizes. For equal size of the dots, the number and the amplitude of the matching effects were more pronounced with ferromagnetic dots. The enhancement of the superconducting properties due to the stray field of the ferromagnetic dots rather than to a local thickness modulation was thus proved. Another significant advance was made by Lange *et al.*,[13] who obtained field-induced superconductivity (FIS) in similar hybrid stuctures, taking advantage of the field compensation of the dots' stray field and the external field. The shift of the corresponding phase diagram $T_c(H)$ takes its origin in the creation of vortex-antivortex pairs (V-AV) in the superconductor due to the stray field of the dots.[19] Gillijns *et al.*[9,10] tuned this field-induced superconductivity by modifying the magnetic state of the ferromagnetic dots. They were able to modify the number of V-AV pairs generated by each dot and, therefore, to shift at will (by discrete steps) the phase diagram up to a maximum value. Nevertheless, this phenomenon was limited to relatively low field (a few mT). Moreover, the works realized until now were mostly performed using lithographically defined dots arrays for which the fabrication is known to be expensive and time-consuming.

In our previous work,[22] we demonstrated the feasibility of an alternative approach to produce magnetic pinning of vortices up to very high fields (2.5 T). Dense arrays of ferromagnetic nanowires can be used to produce magnetic pinning in thin superconducting films. These nanowires are so thin that their diameter is comparable to the magnetic domain wall thickness.[23,24] Therefore, they are single domains, i.e., their magnetization can only lie along the nanowire axis. Moreover, the applied perpendicular magnetic field revealing the matching effects in these superconductor-ferromagnets hybrids is so high that the magnetic state of the nanowires array changes during the measurements. The low-field unsaturated regime should, therefore, be considered separately from the high-field saturated regime. In the latter case, the magnetization of all the nanowires is parallel to the external magnetic field. At low field, the situation is more complex and the magnetization of each nanowire depends not only on the applied magnetic field but also on the magnetic history. Due to the dense packing of the array, the strong dipolar couplings[23] lead to a low remanence and to relatively high saturation fields ($\mu_0 H_s \approx 0.3$ T). Below the saturation field, some nanowires can thus be magnetized antiparallel to the external field. These antiparallel nanowires act as repulsive centers rather than as pinning centers. Moreover, the magnetic state of the array, i.e., the number of pinning and repelling centers, depends on the external field. This last feature noticeably differs from the fixed magnetic state considered in the previously reported studies.

In this paper, our previous study[22] is extended to the case where the ferromagnetic nanowires perforate the superconducting film. New features are observed: first, the first matching field is shifted to lower values when the ferromagnetic nanowires array is not in the saturated state. Moreover, modifying the magnetic history, this first peak can be shifted at will over a certain magnetic field range. Second, the shift of the first matching field goes in hand with an enhancement of the superconducting state. Finally,

field-induced superconductivity is observed up to 1.2 T, i.e., up to the fifth matching field.

The paper is organized as follows: in Sec. II, the experimental details concerning the sample fabrication and measurements are given. This section also refers to the magnetic properties of the Ni nanowires array. Section III is devoted to the low-magnetic-field behavior. The origin of the shift, its tunability, as well as the enhancement of the first matching field are demonstrated. In Sec. IV, the high-magnetic-field-induced superconductivity is analyzed. The possible origins of this effect are discussed. Finally, all the findings are summarized in Sec. V.

II. EXPERIMENTAL

Commercial nanoporous alumina membranes (Synkera Technologies, Inc.) are used to fabricate our superconductor-ferromagnet hybrids. These self-supported membranes are 50 μm thick and have a triangular lattice of pores with an interdistance of 100 nm and a typical ordered domain size of 1 μm^2. The initial pores diameter is about 35 nm. A pore enlargement is performed in order to tune the nanowires diameter. For this purpose, we use sulfuric acid (0.5 M) at 40 °C. The pores enlargement speed is not steady in time but the mean value is about 0.35 nm/min. After enlargement, the membranes are rinsed in pure water. Figure 1(a) shows an alumina membrane with pores of 60 nm in diameter. A 10-nm-thick Cr adhesion layer and a 300-nm-thick Au cathode are then successively evaporated on one face of the membrane. The Ni nanowires are grown in the template using pulsed electrodeposition with −1.05 V for 10 ms and −0.7 V for 90 ms for a total time of about 16 h. The solution used is a Ni sulfate solution 0.5 M. The resulting nanowires are several microns long. The gold cathode is then removed using a [KI 100 g-I_2 27 g]/l solution for 5–10 min at room temperature. The Cr layer is removed by mechanical polishing using silica particles (Syton solution half diluted). The polishing is also used to etch the membrane in order to reveal the nanowires tips. Indeed, the gold penetrates into the pores during the evaporation so the nanowires start to grow several tenths of nm from the surface. This polishing step also guarantees a very good cleaning of the membrane. The surface of the membrane obtained after polishing is shown on Fig. 1(b) (the pores' diameter is 70 nm). A very good filling (>99%) is obtained for enlarged pores. Then, a 20-nm-thick NbN film is deposited on the surface [Fig. 1(c)] through a 4-point transport bridge mask (3.2 mm long and 0.2 mm wide). The reactive sputtering of NbN is performed at room temperature with 8 mtorr of Ar and 0.9 mtorr of N_2 with a setting current of 1 A. The corresponding deposition rate is 8 Å s^{-1} and the power is 370 W. It is worth mentioning that the Ni nanowires tips are slightly oxidized (native oxide), which limits the electrical contact between the ferromagnet and the superconductor. Prior to the NbN deposition the sample's surface was characterized by atomic force microscopy (AFM) measurements. These measurements are presented in Fig. 1(d) (topography of the surface) and Fig. 1(e) [topography along the white line of Fig. 1(d)]. These images reveal an abrupt surface profile (more than 15 nm peak to peak). The maxima correspond to the nanowires' tip and the minima to the alumina surface (between the nanowires). We

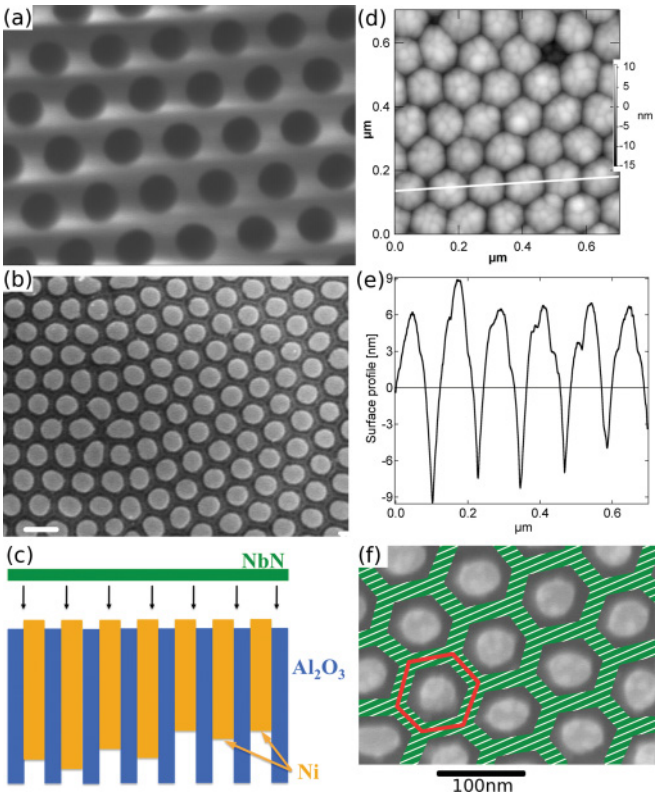

FIG. 1. (Color online) (a) SEM image of the surface of a nanoporous alumina membrane after enlargement of the pores to 60 nm. (b) SEM image of the surface of a nanoporous alumina membrane filled with Ni nanowires (sample NbN70). The white bar at the bottom left corner is 100 nm. (c) Schematic representation of the deposition of a 20-nm-thick superconducting NbN film on top of a filled membrane. (d) Atomic force microscopy image of the surface of NbN70 before the NbN deposition and (e) topography of the surface [along the white line of (d)] showing that the nanowires are more than 15 nm higher than the alumina membrane. (f) Schematic representation of the conducting region of the NbN after deposition on the surface of NbN50 (green-white hatched region) and of the hexagonal unit cell of the array (red).

believed that the interwire region could not be imaged correctly due to the finite size of the AFM tip and that the surface profile is even more pronounced. This rough surface is due to a different polishing speed of the two materials. The deposition of a thin NbN film on such surface allows us to obtain a perforated layer as represented in Fig. 1(f). The conducting region of the NbN deposit corresponds to the white-green hatched region. This is corroborated by the strong increase of the resistivity (about a factor 10) of the NbN deposited on the nanowire array compared to the reference sample (continous NbN deposited on a sapphire substrate).

In this article, we report on three samples with a 20-nm-thick NbN film and nanowires diameter of 50, 60, and 70 nm (respectively named NbN50, NbN60, and NbN70) with characteristics presented in Table I. Each sample has its own reference sample that was deposited simultaneously on a flat sapphire surface. The superconducting properties of the samples are characterized by electrical transport measurements in a ^{4}He cryostat with a temperature stability of about

TABLE I. Samples characteristics.

Sample	T_c (K)	Resistivity (10^{-5} Ωm)	$\xi(0)$ (nm)	$\lambda(0)$ (μm)
NbN50	9.22	6.2	∼1.7	∼2.4
NbN60	9.1	4.2	∼1–2	∼2
NbN70	9.47	4.1	∼1.2	∼2

0.5 mK. The magnetic properties of the Ni nanowires arrays were characterized by both magnetometry [Quantum Design Superconducting Quantum Interference Device (SQUID)] and magnetic force microscopy (MFM) measurements (prior to the NbN deposition).

Figure 2(a) shows the magnetization hysteresis curves of the samples NbN70 and NbN50 at 15 K. In the low-temperature range, the magnetic properties of such Ni nanowires arrays are temperature independent. Major differences are visible between the two samples. The remanence and the coercive field are higher for the smaller diameter sample while the saturation field increases with the diameter of the nanowires. The magnetic state of NbN70 in the remanent state is shown in Fig. 2(b). This figure is the superposition of an AFM and a MFM image at room temperature. The AFM image is the background image and the MFM image has

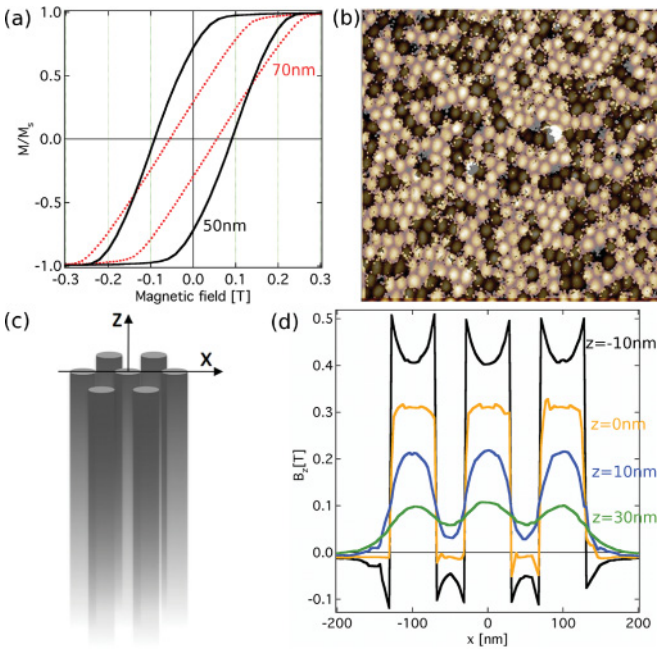

FIG. 2. (Color online) (a) Magnetization hysteresis curves of the samples NbN70 and NbN50 obtained using a SQUID magnetometer. The hysteresis loop deviates more from the ideal square loop as much as the packing of the array increases. (b) MFM image of NbN70 superposed on a AFM image of the same location. The bistable state of the magnetization of the nanowires is clearly observed (either parallel or antiparallel to the nanowires axis). (c) Schematic representation of the seven-nanowire array used for the simulation of the stray magnetic field. The axis system is also represented. (d) The z component of the stray field of the Ni nanowires array represented in (c) for several z values ($z = 0$ nm corresponds to the nanowires' tips).

undergone some basic image treatments. The gray-scale image have been converted to a black-and-white image. The white pixels then have been made transparent while the black pixels have been made white with 50% transparency. This figure reveals the well-known bistable state[23,24] where the Ni nanowires can be in only two magnetic states: homogeneously magnetized along the nanowires axis in both directions. Strong dipolar couplings are present in such systems, leading to a complicated distribution of up- and down-nanowires in small clusters. These strong dipolar couplings are at the origin of the deviation from the expected square loop of isolated nanowires.

The magnetic stray field profile above the nanowires array has been determined using magnetostatic simulations. The simulated array consists of seven Ni nanowires in a triangular arrangement with an interdistance of 100 nm [see Fig. 2(c)]. Similar simulations have been performed with up to 80 nanowires, which leads only to a small decrease in the amplitude of the curves. The diameter (D) of the nanowires used for this calculation amounts to 60 nm and the length (L) is equal to 1.2 μm ($L = 20D$). These values correspond roughly to the sample NbN60 even if the Ni nanowires are probably several microns long. The simulations were performed for different nanowires lengths and revealed that for $L > 10D$, the magnetic field profile is not further modified. The magnetization of each nanowire is fixed at $\vec{M} = (0,0,M_s)$ with $M_s = 5.1 \times 10^5$ A/m, i.e., the typical value for Ni at low temperatures. The z component of the magnetic field above the lattice of nanowires is shown in Fig. 2(d) for different z values ($z = 0$ nm corresponds to the nanowires' tips). The mean-field profile in our sample corresponds approximatively to the $z = -10$ nm case. In this case, the maximum field is about 0.45 T and the minimum field is about −0.07 T. Increasing the z value leads to a rapid drop of the field maximum and of the field modulation amplitude. At $z = 30$ nm, the maximum field reaches hardly 0.1 T and the modulation amplitude is less than 0.05 T. This clearly reveals that the distance between the ferromagnets and the superconducting layer as well as the thickness of the superconductor are critical factors.

III. TUNABLE FIRST MATCHING FIELD

Figure 3 shows the magnetoresistance curve of the sample NbN70 at low resistive states ($R_n \approx 33\,k\Omega$, R_n is the normal state resistivity) which is representative of all the samples' behavior. Many oscillations are observed with a periodicity of about 0.23 T in accordance with the theoretical matching condition for a triangular lattice of pinning centers of interdistance about 100 nm ($H_1 = 0.239$ T). Oscillations are observed in fields up to 3 T in the best samples. These numerous matching effects are due to the large pinning center diameter compared to the coherence length [$\xi(0) \approx 1.3$ nm] that allows us to pin giant vortices.

In this section, we focus on the low-magnetic-field ($0 \leqslant H \leqslant H_1$) behavior of our samples. In fact, the first positive matching effect is dependent on the magnetic-field history. Indeed, when the magnetization of the ferromagnetic nanowires array is not at its saturation value, the first matching field is reduced compared to its theoretical value. This is illustrated in

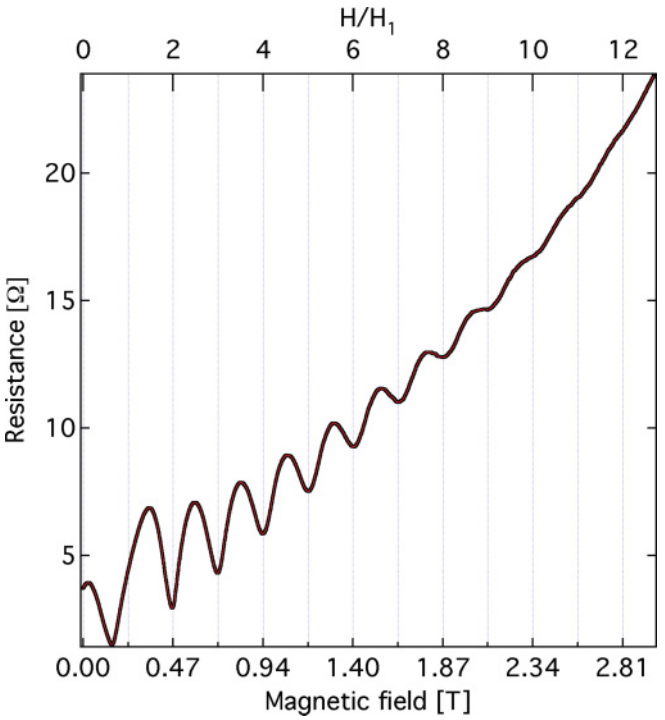

FIG. 3. (Color online) Magnetoresistance curve of the sample NbN70 at 7.1 K ($0.75 \times T_c^{\text{mid}}$) obtained by applying a dc current $I = 10\ \mu$A. Numerous oscillations reminiscent of matching effects are observed. The matching fields nicely fit the theoretical ones (multiple of $H_1 = 0.239$ T). The field is swept from zero (in the remanent state) to positive values (black arrow).

Fig. 4(a), which compares the magnetoresistance curve of the NbN70 sample obtained by sweeping the magnetic field from the negative to the positive saturation (solid curve) and from the positive saturation to zero field (dashed curve). When coming from positive saturation, the first matching dip is located at its theoretical value. On the contrary, when coming from negative saturation, it is located at a lower value $H_1^* \approx 0.6H_1$. Surprisingly, in this latter case, the resistance is lower, i.e., the superconducting state is reinforced.

A. Origin of the shift of the first matching field

The so-called matching effect occurs in a superconductor when the vortex lattice "matches" the pinning center lattice. As the periodicity and the symmetry of the nanowires array cannot be modified, the shift observed in Fig. 4(a) should come from a reduction of the number of pinning centers. Indeed, due to the strong dipolar coupling, some nanowires can have their magnetization antiparallel to the external magnetic field at low field. In this case, the number of pinning centers is reduced. As the number of pinning centers is dependent on the magnetic history, the matching field is also history dependent.

The position of the first matching field can be precisely determined from the magnetization hysteresis of the array. If one considers a unit cell of the lattice, the matching condition, for which the number of vortices is equal to the number of pinning centers, becomes for positive fields:

$$f_{\text{up}} = f_v, \tag{1}$$

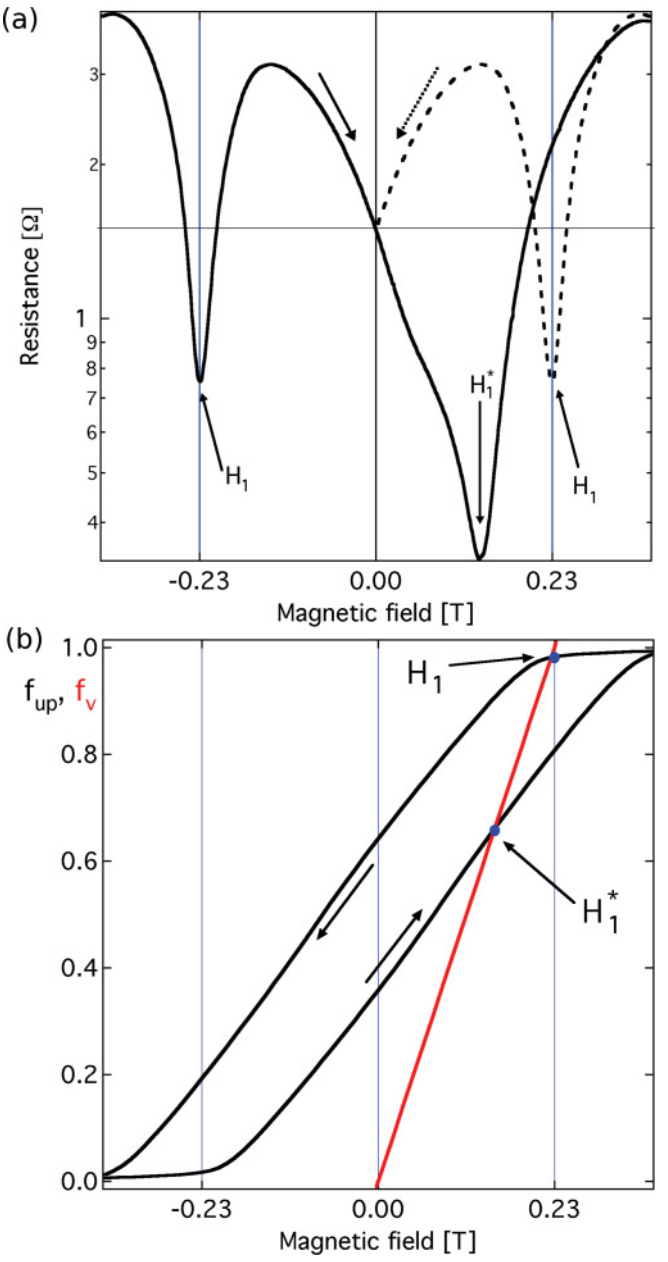

FIG. 4. (Color online) (a) Close-up of the low-field behavior of the magnetoresistance curve of the sample NbN70 at 7.1 K ($0.75 \times T_c^{\text{mid}}$) (Fig. 3). The black curve is obtained starting from negative saturation and the dashed curve from the positive one. (b) Evolution of the fraction of the ferromagnetic nanowires whose magnetization is parallel to a positive external magnetic field (f_{up}, black curve) and of the fraction of vortices per unit cell (f_v, red line) with respect to the external magnetic field. f_{up} is extracted from SQUID measurements at 15 K [Eq. (3)]. The intersection of f_{up} and f_v are in qualitative agreement with the experimentally found minima at H_1^* and H_1 in Fig. 4(a).

where f_{up} is the "fraction" of nanowires per unit cell parallel to a positive external field and f_v is the fraction of vortex per unit cell [see Fig. 1(f)]. The value for f_{up} can be extracted from the magnetization $M(H)$ of the nanowires array that was obtained by SQUID measurements at low temperature. Indeed, given

that the nanowires' magnetization has only two orientations, one has:

$$\frac{M(H)}{M_s} = f_{\mathrm{up}}(H) - f_{\mathrm{down}}(H), \tag{2}$$

where M_s is the magnetization at saturation and f_{down} is the fraction of repulsive centers (i.e., the fraction of nanowires per unit cell antiparallel to the positive external field). Knowing that $f_{\mathrm{up}}(H) + f_{\mathrm{down}}(H) = 1$, Eq. (2) becomes:

$$f_{\mathrm{up}}(H) = \frac{1}{2}\left[1 + \frac{M(H)}{M_s}\right]. \tag{3}$$

On the other hand, the fraction of vortex per unit cell is well approximated by

$$f_v(H) = \frac{H}{H_1}, \tag{4}$$

where $H_1 = 0.23$ T in our case. The evolutions of $f_{\mathrm{up}}(H)$ and $f_v(H)$ are sketched in Fig. 4(b). The black curve corresponds to the $f_{\mathrm{up}}(H)$ cycle while the red straight line corresponds to $f_v(H)$. The intersections of these two curves give the solutions of the Eq. (1) (the matching conditions). Contrary to the usual experiments with pinning centers arrays, there are here two solutions for the first matching condition because the number of pinning centers is not fixed. The first one is realized at $f_{\mathrm{up}} = 1$, i.e., when all the nanowires are in the saturated state. As the positive saturation is maintained down to about 0.1 T, it is possible to observe the matching effect at its theoretical value, namely $H_1 = 0.23$ T. It is the classical matching effect corresponding to the triangular lattice of pinning centers with interspace about 100 nm. Starting at negative saturation and sweeping to positive fields, the matching condition is fulfilled at $H_1^* \approx 0.14\,\mathrm{T} < H_1$ [see Fig. 4(b)]. The minimum of resistance reported on Fig. 4(a) is in qualitative agreement with the intersection of the f_v and f_{up} curves shown on Fig. 4(b).

It is worth mentioning that our results differ from the predictions made by Reichhardt *et al.*[25] for diluted arrays of pinning centers. Indeed, using molecular dynamics it is found that the matching field is robust on the random removal of pinning centers. Also, experiments with Fibonacci arrays[26] corroborate the above simulations, i.e., local matching prevails when different matching geometries are present. By contrast, the pinning centers are replaced in our case by repelling centers that prevent to maintain the overall triangular arrangement of the vortex lattice.

B. Origin of the superconductivity enhancement at H_1^*

This enhanced superconductivity manifests itself through a lower resistive state at H_1^* than at H_1. This enhancement occurs for low resistive states, it is, therefore, related to the vortices' depinning and motion. Two factors influencing the vortex motion and the vortex pinning are competing at H_1^*. First, the vortex lattice is not perfectly ordered due to the repelling centers. Therefore, the vortex-vortex interaction force is not zero, contrary to the case at H_1 where it is canceled two by two due to the triangular symmetry. This term leads to a lower depinning current compared to a perfectly ordered array of pinning centers. Second, the repelling centers act as barriers for the vortex motion. The presence of such barriers around the pinning centers increases, the critical depinning force and hinders the vortex motion, leading to a reduced vortex channeling.[27] One of these competing factors will prevail depending on the relative intensity of the pinning force and of the vortex-vortex interaction force. For the particular sample shown in Fig. 4(a), the pinning force clearly overcomes the vortex-vortex interaction force. Actually, such lower resistive state at H_1^* was observed only for superconducting films perforated by the nanowires. This is due to the enhanced magnetic pinning compared to the case without perforation, for which the magnetic-field modulation is much less pronounced [see Fig. 2(d)].

The latter considerations are highlighted by the local magnetic state of the nanowires' array shown in Fig. 2(b). This MFM image (see Sec. II for details) reflects the potential landscape felt by the vortices. It reveals that the pinning centers are not randomly distributed due to the strong interwire dipolar coupling in the array. Therefore, the pinning centers form clusters separeted by clusters of repelling nanowires. The vortices motion is clearly hindered by such disordered distribution of barriers.

Furthermore, this enhancement of the superconducting properties at H_1^* compared to H_1 is in agreement with previous theoretical works. Notably, Chen *et al.*[27] compared theoretically the critical current of a thin superconducting film in close proximity with ferromagnetic dots in parallel and antiparallel magnetization alignment. The antiparallel arrangement produces a larger critical current of the superconducting film than the ferromagnetic one. This result is qualitatively similar to the one reported in the present work. Moreover, it has been also proved numerically[25,28,29] and experimentally[30–32] that partly disordered lattices[25] or quasiperiodic[28,29] pinning arrays exhibit enhanced superconducting properties compared to perfectly periodic arrays and randomly distributed pinning centers.

C. Tunability of the matching-field shift

From Fig. 4, one sees that varying the magnetic configuration of the bistable nanowires array allows us to tune the position of the first matching dip. The allowed matching fields lie in the interval $[H_1^*, H_1]$ that corresponds to the intersection between the function $f_v(H)$ and the two major branches of the function $f_{\mathrm{up}}(H)$. As the magnetic state of the nanowires array [or equivalently the $f_{\mathrm{up}}(H)$ curve] can be modified by performing minor cycles, intermediate values between the two major branches can thus be reached. Figure 5(a) shows that the matching condition may be realized at any intermediate magnetic field between H_1 and H_1^* by performing such minor cycles. This leads to a tunable shift of the first matching peak as seen on Fig. 5(b). Intermediate values of resistance at the matching conditions are also reached. These intermediate resistive states are directly related to the number of repelling centers obtained in these minor cycles. Therefore, modifying the magnetic history allows us to tune at will the first matching-field position and intensity in a range given by the magnetic properties of the nanowires array.

Figure 5(c) shows the evolution of the experimentally obtained first matching fields as a function of f_{up}. The blue

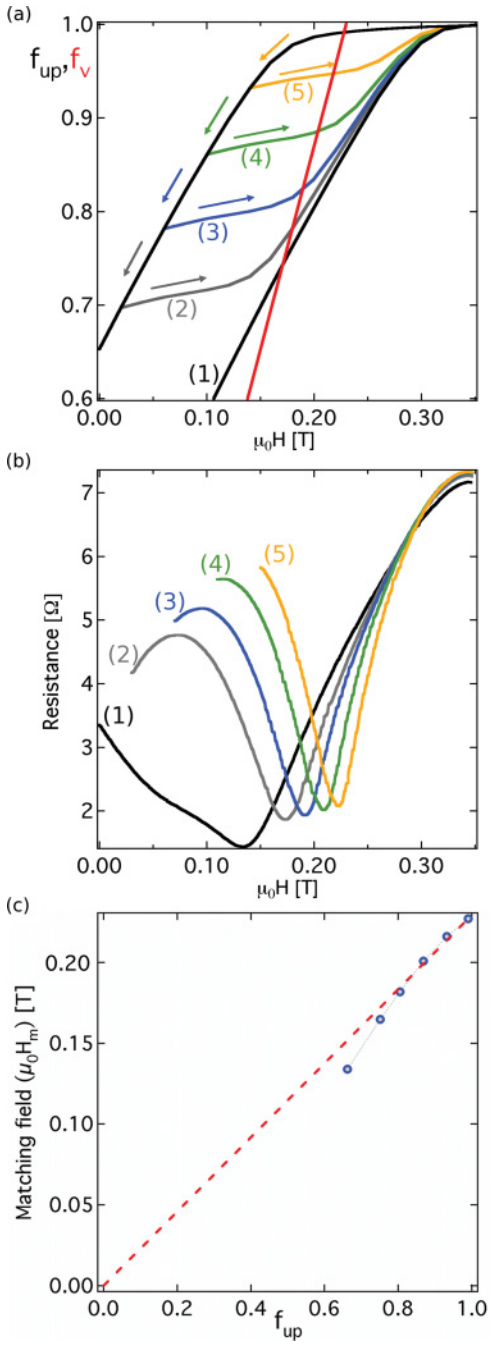

FIG. 5. (Color online) (a) Minor cycles in the hysteretic loop of the fraction of pinning centers (f_{up}) of NbN70 obtained by sweeping the external magnetic field back and forth from the positive saturation to different low field values. The intersection between f_{up} and the fraction of vortex per unit cell f_v (red straight line) depends on the minor cycle. (b) Magnetoresistance curves obtained from the negative saturation to the positive one (black curve) and for the four minor cycles depicted in (a) performed at 7.1 K ($0.75 \times T_c^{mid}$). One observes that the matching field can be adjusted at will between H_1 and H_1^*, in agreement with the intersections between f_{up} and f_v. (c) Evolution of the matching field as a function of f_{up}. The matching field was extracted from the magnetoresistance curves and f_{up} from the hysteresis curves. The blue dots corresponds to the experimental data and the dashed line to the theoretical behavior corresponding to $f_v = f_{up}$ (in this case $\mu_0 H_m = 0.23 \times f_{up}$).

dots correspond to the experimental data and the dashed line to the expected behavior corresponding to $f_v = f_{up}$. A good agreement is found for $f_{up} > 0.8$ (i.e., for a relatively low concentration of repelling centers). The deviations shown for $f_{up} < 0.8$ are related to the presence of a large concentration of repelling centers that induce disorder in the pinning center lattice. Therefore, as observed by Rosen *et al.*,[33] the matching field is reduced compared to its theoretical value.

D. Influence of the nanowires diameter

The influence of the nanowires diameter (for a fixed nanowires interdistance) on the matching field shift is now discussed. As shown in Sec. II, the larger the diameter, the lower the remanence and the higher the saturation field. Therefore, considering different nanowire diameterd, their magnetic behavior will have a different impact on the superconducting properties and particularly on the first matching shift. Several samples have been studied with nanowires diameter ranging from 40 to 70 nm. It has been experimentally observed that the larger the diameter, the larger the first matching peak shift. Figure 6(a) shows the evolution of the first matching field as a function of the initial magnetic field of minor loops for different nanowire diameter. For wire diameter of 40 nm, no shift of the first matching field is observed. Indeed, $H_1^* = H_1$ for all the minor loops because the saturation field is lower than H_1. For diameters larger than 40 nm, the saturation field is larger than H_1 and thus a shift of the matching field is observed. This shift is more pronounced for the bigger nanowires because of their larger saturation field. Therefore, the intersection of $f_{up}(H)$ and $f_v(H)$ takes place at lower field.

The sample NbN50 (diameter 50 nm) is of particular interest. Indeed, as shown in Fig. 6(a), the matching condition is only realized very close to the saturation field. This should lead to a very small shift of the first matching peak, i.e., $H_1^* \sim 0.95 H_1$. Figure 6(b) shows the magnetoresistance curves of NbN50 for different minor cycles. As expected, the first matching effect is almost not shifted. However, an intermediate dip appears at low field (H_i). It is positioned close to zero for the major branch, shifts to a higher field, and progressively vanishes as smaller minor cycles are performed. These matching effects do not correspond to a matching condition [see Fig. 6(a)]. Indeed, at these fields, the number of pinning centers somewhat exceeds the number of vortices. Nevertheless, we believe that these minima can be ascribed to matching effects, due to the close proximity of the two curves and the experimental error. The discrepancy from the theory could also come from an additional fraction of nonactive pinning sites resulting from the huge amount of repelling centers present close to zero field. This clearly reflects the strong and complicated magnetic interaction between the superconducting film and the Ni nanowires array that leads to a low resistive state at a somewhat unexpected magnetic field. Therefore, both minima (H_1 and H_i) can be considered as first matching effect, in the sense that there is only one vortex captured by active pinning center in both cases. In this point of view, there are two successive first matching fields. Both first matching effects are tunable, but the one at 0.23 T is tunable only in a very narrow range (several percentage points). This unique feature is due to the proximity

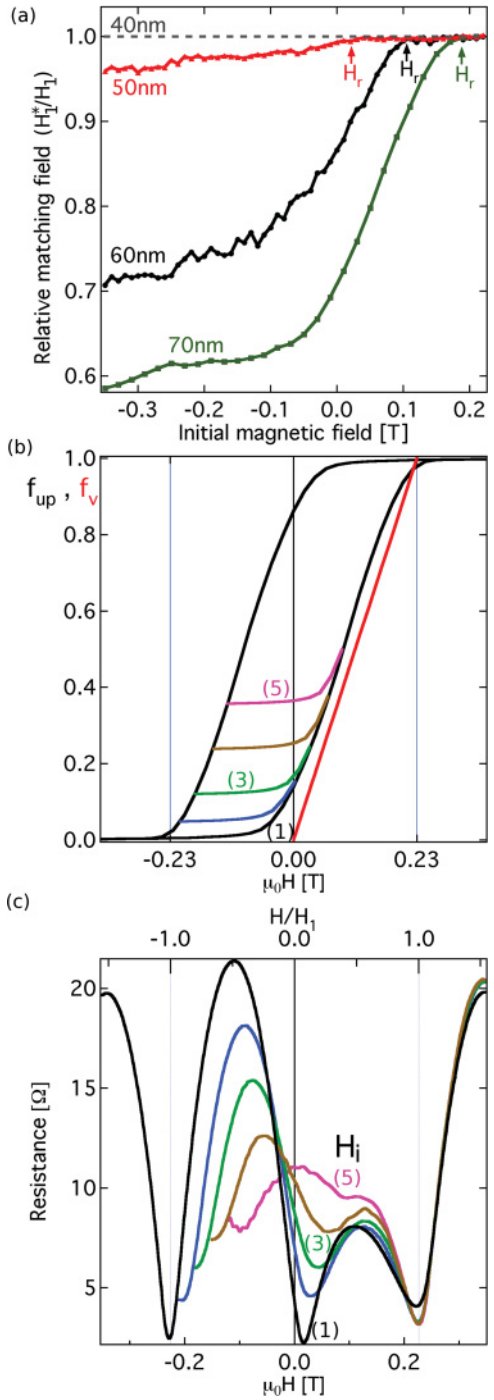

FIG. 6. (Color online) (a) Evolution of the first matching field as a function of the initial magnetic field of minor loops for different nanowire diameter. (b) Fraction of pinning centers per unit cell ($f_{\rm up}$, black curve) and fraction of vortex per unit cell (f_v, red line) as a function of the external magnetic field for different minor loops (sample NbN50). (c) Magnetoresistance curves at 7.1 K ($0.77 \times T_c^{\rm mid}$) with the same minor loops as in (b) (sample NbN50). A tunable matching effect (H_i) is obtained very close to zero field in addition to the one present at the geometrical first matching field H_1, although the condition $f_{\rm up} = f_v$ is not fulfilled.

of the $f_{\rm up}$ and f_v curves. It is also worth noting that if the $f_{\rm up}$ and f_v curves were coinciding in some field range, some kind of continuous matching effect would happen. By fine-tuning the magnetic properties of our array (packing), it may be possible to realize this unique behavior.

IV. MISLEADING FIELD-INDUCED SUPERCONDUCTIVITY

In this section, the field-induced superconductivity observed in our samples is discussed. Figure 7 shows the phase diagram of the sample NbN60. The black solid curve corresponds to the critical depinning temperature, i.e., the temperature at which the vortices start to move. This curve was obtained by adjusting the temperature in order to maintain the sample resistance at a fixed criterion, just above the perfect superconducting state (namely 10^{-4} R_n with R_n the normal state resistance). The resistance was measured by applying a direct current of 20 μA, which is much lower than the instability current at these temperatures (several mA). The critical depinning temperature is larger than the zero-field value in several magnetic field intervals which is, by definition, field-induced superconductivity. The critical temperature curve of the reference sample (deposited simultaneously on a flat sapphire substrate) is presented on the same figure (dashed red curve). In order to compare the curves' shape, the critical temperatures have been normalized to their zero-field values (7.16 K for NbN60 and 9.94 K for its reference sample).

The blue region (R) corresponds to the resistive state (vortex motion), the orange region (S) corresponds to the perfect superconducting state (motionless vortices). Numerous oscillations

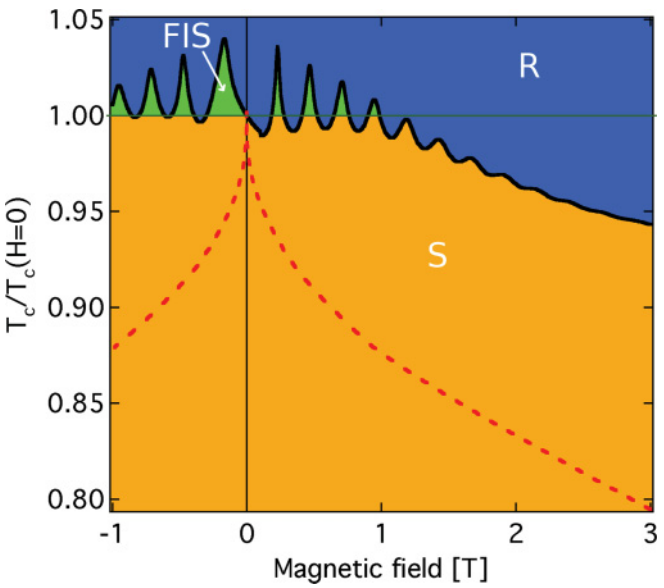

FIG. 7. (Color online) Phase diagram of superconductivity for the sample NbN60 (black solid line) and its reference sample grown simultaneously on sapphire (red dashed line). The criterion is the appearance of resistance ($10^{-4} \times R_n$). The temperatures are normalized with respect to the zero field value (7.16 K and 9.88 K for NbN60 and its reference sample, respectively). The measurements were performed from positive to negative fields. The blue region (R) corresponds to the resistive state ($R > 10^{-4} \times R_n$), the green region (FIS) corresponds to field-induced superconductivity ($R < 10^{-4} \times R_n$), and the orange (S) region corresponds to the perfect superconducting state of NbN60 ($R < 10^{-4} \times R_n$).

are observed, due to matching effects between the vortices and the triangular lattice of ferromagnetic nanowires.[22] The overall shape of the transition line differs noticeably from the reference sample, i.e., the superconductor-ferromagnet hybrid sample is clearly less affected by the external magnetic field. The green region (FIS) is the field-induced superconductivity region (motionless vortices). These regions mainly correspond to the matching conditions (peaks). For this particular sample, the field-induced superconductivity is observed up to 1.2 T, i.e., up to the fifth matching field.

Many experimental and theoretical papers have already considered field-induced superconductivity and we have observed it at high magnetic fields. The origin of this phenomenon is generally associated to the presence of V-AV pairs in the superconducting thin film.[9,13] These V-AV pairs are due to the stray fields of the ferromagnetic dots. An antivortex is always associated with a vortex due to the magnetic flux conservation. This leads to a global shift of the phase diagram to a magnetic field $H = nH_1$,[9,10,12,21] with n being the number of V-AV pairs generated by each dot. It has been experimentally observed that the appearance of a V-AV pair requires that the magnetic flux produced on top of the dot roughly exceeds one quantum of flux ϕ_0.[9] In this case, a vortex is created above the dot and an antivortex between the dots. On the other hand, simulations were performed by Milosevic *et al*.[21] on a sample with ferromagnetic dots on top of a superconducting film. A rich variety of states has been revealed by calculating the zero-field superconducting ground state as a function of the magnetization and as a function of the ratio between the dots interdistance and the coherence length. One important result of their work is that the transition line between the ground state with and without a V-AV pair corresponds to a magnetic flux above each ferromagnetic dot equal to $1.29\phi_0$. More generally, it was roughly found that the appearance of N vortex-antivortex pairs requires that the magnetic flux above the dot (in the film) is more than $N \times \phi_0$. From the results of Fig. 2(d), the magnetic flux above each nanowire is $\phi_{NW} = 0.45\,T \times S_{NW} = 0.61\phi_0$ (S_{NW} is the surface of the nanowires' tip). This value is much lower than the $1.29\phi_0$ threshold found by Milosevic *et al*. This means that, in our case, the dots do not create any V-AV pair. Moreover, a V-AV appears if the magnetic flux between the nanowires (ϕ_{AAO}) is opposite to the one above the dots and also equal to $1.29\phi_0$. This is clearly not the case here because $\phi_{AAO} = 0.29\phi_0$. These considerations lead to the conclusion that the FIS observed here is not related to V-AV pair creation. In our case, field-induced superconductivity neither manifests itself neither as a broad region of enhanced T_c nor as a global shift of the phase diagram but rather as localized enhanced T_c region corresponding to the matching effects. Therefore, the FIS presented here seems to originate from the disappearance of the zero-field peak (due to the modification of the magnetic state of the array at zero field compared to high fields) rather than in the shift of the phase diagram. Further investigations will be carried out in order to clarify the origin of this misleading FIS.

V. CONCLUSION

The superconducting properties of NbN thin films perforated by an array of ferromagnetic nanowires have been studied. Strong matching effects have been observed up to 3 T. The first matching field is reduced from its theoretical value H_1 when the ferromagnetic nanowires array is not in the saturated state ($H_1^* < H_1$). Moreover, the first matching field shift is accompanied by an enhancement of the superconducting state compared to H_1. This is due to the presence of the repelling centers (nanowires magnetized antiparallel to the external field) that act as barriers, leading to an increase of the net pinning force and a decrease of the vortex channeling. The shift of the first matching field can be tuned between the theoretical (H_1) and a lower matching field (H_1^*) by performing minor loops into the main hysteresis curve. The diameter of the nanowires strongly influences the shift of the matching effect since it modifies the magnetization curve of the nanowires array. For the smallest diameter (50 nm), an additional resistance minimum appears well below the first matching field. Interestingly, field-induced superconductivity is observed up to 1.2 T in the best samples. This high field-induced superconductivity cannot originate from V-AV pairs formation. Indeed, magnetostatic simulations revealed that the magnetic field profile into the superconducting layer is not suitable even for one vortex-antivortex pair formation.

ACKNOWLEDGMENTS

X. H. is a Research Fellow of the National Fund for Training in Research in Industry and Agriculture (FRIA), Belgium. S. A. is a Research Fellow of the National Fund for Scientific Research (FNRS), Belgium. This work was partly supported by the Interuniversity Attraction Pole Program (P6/42), Belgian State, Belgian Science Policy and by the Methusalem Funding. The authors thank B. Nysten (Université catholique de Louvain, Institute of Condensed Matter and Nanosciences) for the AFM measurements and W. Gillijns for some AFM, MFM, and SQUID measurements.

*xavier.hallet@uclouvain.be

[1] A. I. Buzdin, Rev. Mod. Phys. **77**, 935 (2005).
[2] A. Y. Aladyshkin, A. V. Silhanek, W. Gillijns, and V. V. Moshchalkov, Supercond. Sci. Technol. **22**, 053001 (2009).
[3] I. F. Lyuksyutov and V. L. Pokrovsky, Adv. Phys. **54**, 67 (2005).
[4] M. Vélez, J. Martín, J. Villegas, A. Hoffmann, E. González, J. Vicent, and I. K. Schuller, J. Magn. Magn. Mater. **320**, 2547 (2008).
[5] V. V. Moshchalkov and J. Fritzsche, *Nanostructured Superconductors* (World Scientific Publishing, 2011).
[6] Y. Otani, B. Pannetier, J. Nozières, and D. Givord, J. Magn. Magn. Mater. **126**, 622 (1993).

[7]D. J. Morgan and J. B. Ketterson, Phys. Rev. Lett. **80**, 3614 (1998).
[8]A. Hoffmann, P. Prieto, and I. K. Schuller, Phys. Rev. B **61**, 6958 (2000).
[9]W. Gillijns, A. V. Silhanek, and V. V. Moshchalkov, Phys. Rev. B **74**, 220509 (2006).
[10]W. Gillijns, M. V. Milošević, A. V. Silhanek, V. V. Moshchalkov, and F. M. Peeters, Phys. Rev. B **76**, 184516 (2007).
[11]A. V. Silhanek, W. Gillijns, V. V. Moshchalkov, V. Metlushko, F. Gozzini, B. Ilic, W. C. Uhlig, and J. Unguris, Appl. Phys. Lett. **90**, 182501 (2007).
[12]A. V. Silhanek, W. Gillijns, M. V. Milošević, A. Volodin, V. V. Moshchalkov, and F. M. Peeters, Phys. Rev. B **76**, 100502 (2007).
[13]M. Lange, M. J. Van Bael, Y. Bruynseraede, and V. V. Moshchalkov, Phys. Rev. Lett. **90**, 197006 (2003).
[14]Z. Yang, M. Lange, A. Volodin, R. Szymczak, and V. V. Moshchalkov, Nat. Mater. **3**, 793 (2004).
[15]S. Haindl, M. Weisheit, T. Thersleff, L. Schultz, and B. Holzapfel, Supercond. Sci. Technol. **21**, 045017 (2008).
[16]J. E. Villegas, C.-P. Li, and I. K. Schuller, Phys. Rev. Lett. **99**, 227001 (2007).
[17]M. J. Van Bael, J. Bekaert, K. Temst, L. Van Look, V. V. Moshchalkov, Y. Bruynseraede, G. D. Howells, A. N. Grigorenko, S. J. Bending, and G. Borghs, Phys. Rev. Lett. **86**, 155 (2001).
[18]I. F. Lyuksyutov and V. Pokrovsky, Phys. Rev. Lett. **81**, 2344 (1998).
[19]M. V. Milošević, S. V. Yampolskii, and F. M. Peeters, Phys. Rev. B **66**, 174519 (2002).
[20]I. K. Marmorkos, A. Matulis, and F. M. Peeters, Phys. Rev. B **53**, 2677 (1996).
[21]M. V. Milošević and F. M. Peeters, Phys. Rev. Lett. **93**, 267006 (2004).
[22]X. Hallet, M. Mátéfi-Tempfli, S. Michotte, L. Piraux, J. Vanacken, V. V. Moshchalkov, and S. Mátéfi-Tempfli, Appl. Phys. Lett. **95**, 252503 (2009).
[23]K. Nielsch, R. B. Wehrspohn, J. Barthel, J. Kirschner, U. Gösele, S. F. Fischer, and H. Kronmüller, Appl. Phys. Lett. **79**, 1360 (2001).
[24]K. Nielsch, R. Wehrspohn, J. Barthel, J. Kirschner, S. Fischer, H. Kronmüller, T. Schweinböck, D. Weiss, and U. Gösele, J. Magn. Magn. Mater. **249**, 234 (2002).
[25]C. Reichhardt and C. J. Olson Reichhardt, Phys. Rev. B **76**, 094512 (2007).
[26]J. E. Villegas, M. I. Montero, C.-P. Li, and I. K. Schuller, Phys. Rev. Lett. **97**, 027002 (2006).
[27]Q. H. Chen, G. Teniers, B. B. Jin, and V. V. Moshchalkov, Phys. Rev. B **73**, 014506 (2006).
[28]V. Misko, S. Savel'ev, and F. Nori, Phys. Rev. Lett. **95**, 177007 (2005).
[29]V. R. Misko, S. Savel'ev, and F. Nori, Phys. Rev. B **74**, 024522 (2006).
[30]A. V. Silhanek, W. Gillijns, V. V. Moshchalkov, B. Y. Zhu, J. Moonens, and L. H. A. Leunissen, Appl. Phys. Lett. **89**, 152507 (2006).
[31]M. Kemmler, C. Gürlich, A. Sterck, H. Pöhler, M. Neuhaus, M. Siegel, R. Kleiner, and D. Koelle, Phys. Rev. Lett. **97**, 147003 (2006).
[32]M. Kemmler, D. Bothner, K. Ilin, M. Siegel, R. Kleiner, and D. Koelle, Phys. Rev. B **79**, 184509 (2009).
[33]Y. J. Rosen, A. Sharoni, and I. K. Schuller, Phys. Rev. B **82**, 014509 (2010).